Computers and Electrical Engineering 133 (2026) 111076

Contents lists available at ScienceDirect

Computers and Electrical Engineering

journal homepage: www.elsevier.com/locate/compeleceng

Attention-guided electroencephalography fusion with fractal and nonlinear dynamics decodes early Alzheimer's biomarkers

Chayut Bunterngchit [a,b], Chaowanan Jamroen [c], Saba Aslam [d], Abdur Rasool [e,f], Oluwarotimi Williams Samuel [g,*]

[a] Division of Industrial and Logistics Engineering Technology, Faculty of Engineering and Technology, King Mongkut's University of Technology North Bangkok, Rayong Campus, Rayong 21120, Thailand
[b] State Key Laboratory of Multimodal Artificial Intelligence Systems, Institute of Automation, Chinese Academy of Sciences, Beijing 100190, China
[c] Division of Electrical and Automation Engineering Technology, Faculty of Engineering and Technology, King Mongkut's University of Technology North Bangkok, Rayong Campus, Rayong 21120, Thailand
[d] Shenzhen Institutes of Advanced Technology, Chinese Academy of Sciences, Shenzhen 518055, China
[e] Department of Information and Computer Sciences, University of Hawaii at Manoa, Honolulu HI, 96822, USA
[f] Department of Statistics and Data Science, Southern University of Science and Technology, Shenzhen 518055, China
[g] University of Derby, Data Science Research Centre, College of Science & Engineering, Derby DE22 3AW, United Kingdom

ARTICLE INFO

Dataset link: https://github.com/yiamcb/GAEF

Keywords:
Deep learning
EEG
Attention mechanisms
Alzheimer's disease
Fractal dynamics
Nonlinear EEG analysis

ABSTRACT

Alzheimer's disease (AD) presents a critical and growing challenge to healthcare systems due to its neurodegenerative nature and its complex, varied effects on cognitive function. Although electroencephalography (EEG) data combined with deep learning methods have shown promise for early detection, existing approaches often struggle to achieve reliable accuracy. This difficulty arises from the subtle and heterogeneous neural patterns associated with AD progression, as well as the heightened risk of overfitting when working with small or imbalanced datasets. To address these limitations, this study introduces a new diagnostic modeling paradigm: the gated recurrent unit–attentive EEG fusion (GAEF) model, designed to effectively capture both spectral and temporal dependencies in EEG data. The GAEF model incorporates an attention mechanism that enhances the model's focus on the most relevant patterns for distinguishing AD, frontotemporal dementia (FTD), and cognitive normal (CN) cases. Furthermore, the model leverages advanced features rooted in fractal and nonlinear dynamics, including Higuchi fractal dimension and Lyapunov exponents, alongside spectral entropy and power spectral density across various EEG bands, to improve classification boundaries. Experimental results across multiple standard datasets demonstrate the robust generalization capability of the GAEF model, achieving a 98.3% accuracy across AD, FTD, and CN classes in both training and testing without overfitting. These findings underscore the model's practical suitability for reliable deployment in real-world clinical scenarios, significantly advancing precision in AD diagnosis, facilitating early detection, and enhancing patient care strategies.

* Corresponding author.
E-mail address: o.samuel@derby.ac.uk (O.W. Samuel).

https://doi.org/10.1016/j.compeleceng.2026.111076
Received 12 July 2025; Received in revised form 19 January 2026; Accepted 21 February 2026
Available online 3 March 2026
0045-7906/© 2026 Published by Elsevier Ltd.

1. Introduction

Alzheimer's disease (AD) has emerged as a formidable challenge for healthcare systems over the past few decades [1]. This neurodegenerative disorder significantly impairs cognitive functions and is currently recognized as the predominant form of dementia. It is estimated that over 55 million people suffer from dementia worldwide [2]. The projected healthcare costs for long-term AD care are staggering, potentially reaching 1 trillion USD by 2050 [3].

Beyond its cognitive impact, AD can be fatal, with dementia ranked as the seventh leading cause of death and AD accounting for 60%–70% of cases [3]. The disease imposes a substantial burden not only on patients but also on caregivers and society at large. AD manifests through a wide spectrum of cognitive and behavioral symptoms. Initially, patients experience subtle issues such as mild memory loss and cognitive impairments, with individuals noticing minor deterioration in their cognitive functions [4]. As the disease progresses, these symptoms lead to increased disruptions in daily activities. AD profoundly impacts cognitive processes, affecting fundamental mechanisms essential for memory formation, attention control, and information processing [5]. Neurobiological studies have revealed pathological mechanisms associated with AD, particularly the accumulation of amyloid-beta plaques and tau protein tangles in the brain [6]. These abnormalities can trigger synaptic dysfunction and neuronal loss, leading to cognitive deficits that emerge from disrupted neural circuits responsible for memory consolidation, retrieval, and integration. This comprehensive impact underscores the critical need for early detection and effective management strategies for AD.

Detecting AD presents significant challenges due to the heterogeneity of symptoms across individuals [7]. To address this complexity, a variety of clinical and non-clinical methods have been developed, leveraging multidisciplinary approaches including clinical testing, neuropsychological assessments, and neuroimaging. Conventional clinical evaluations for AD are guided by established frameworks such as the diagnostic and statistical manual of mental disorders [8] and the National Institute on Aging and Alzheimer's Association (NIA-AA) criteria [9]. These assessments typically involve the review of medical history, physical examination, and analysis of cognitive function using instruments like mini-mental state examination (MMSE) [10] or Montreal cognitive assessment [11]. Additionally, these evaluations may include assessments of instrumental activities of daily living to identify functional impairments. Neuropsychological assessments are also conducted to analyze specific cognitive domains affected by AD, including, memory, language attention, and visuospatial abilities. Various specialized tests, such as the Wechsler memory scale and the trail-making test, are employed to detect cognitive deficits associated with AD [12]. These comprehensive assessment approaches aim to provide a thorough evaluation of an individual's cognitive status and functional capabilities, facilitating early detection and accurate diagnosis of AD.

Beyond conventional clinical assessments, various non-invasive methods have gained prominence for early detection and differential diagnosis of AD. Brain–computer interfaces, particularly those using electroencephalography (EEG), have emerged as promising tools in AD research. EEG's non-invasive nature and high temporal resolution make it invaluable for capturing dynamic neural activity patterns associated with cognitive impairments [13–15]. This approach offers unprecedented insights into the neural underpinnings of cognitive decline in AD, enhancing our understanding and potentially leading to novel diagnostic and therapeutic strategies.

EEG is a neuroimaging technique that records electrical activity generated by neurons in the brain. Its ability to capture dynamic changes in neural activity makes EEG particularly valuable for detecting subtle signs of cognitive decline. EEG can reveal distinct patterns associated with aberrant neural oscillations, which are characteristic of disruptions in individuals with AD [16]. Key EEG biomarkers for AD include the alterations in resting-state rhythms and the changes in event-related potentials (ERPs). These biomarkers not only reflect underlying neuropathological changes but also provide insights into disease progression and functional impairments. The diagnostic potential of EEG has been significantly enhanced by advancements in signal processing techniques and the application of machine learning (ML) algorithms. These sophisticated methods have improved the ability to differentiate between healthy individuals and those with cognitive impairments.

While EEG does face challenges related to signal variability, the integration of advanced analytical methods has substantially improved its diagnostic accuracy. This enhanced capability not only improves detection rates but also supports the development of more effective clinical management strategies for AD. As a result, EEG has become an increasingly valuable tool in the early detection and monitoring of AD. Notably, the integration of features derived from fractal and nonlinear dynamics has further enhanced the diagnostic capability of EEG-based models by capturing complex temporal irregularities and chaotic behavior in brain activity, which are often indicative of early-stage AD.

The existing works summarized in Section 2 provide a solid foundation for early AD detection using EEG data and deep learning (DL) methods. However, the accuracy of these methods has been limited due to the heterogeneity of disease-capturing patterns. Moreover, many of these models are computationally complex and lack robustness across diverse real-world settings, which hampers their clinical applicability. Given that AD treatment relies heavily on accurate and practical detection tools, even a high classification rate raises concerns that may lead clinicians to favor conventional detection methods.

Accuracy and precision are crucial for DL models to instill confidence in clinicians regarding the results. Achieving high precision is challenging due to the wide range of disease symptoms across subjects, from subtle to apparent. Consequently, determining generalized decision boundaries is of utmost importance. Furthermore, existing models show performance variability across different datasets, suggesting potential overfitting or poor generalizability.

To address these challenges, this study proposes a robust method called the gated recurrent unit (GRU) attentive EEG fusion (GAEF) model, which leverages a GRU-based attention mechanism to effectively capture nuanced patterns in EEG data by simultaneously modeling both spectral and temporal dependencies, a novel approach to characterizing AD. The integration of the duo (temporal and spectral features) provide additional discriminatory power in differentiating AD from other dementia subtypes.

This method enhances brain activity analysis, enabling more accurate distinction between AD and non-AD cases. The study utilizes multiple EEG data from open source AD datasets and emphasizes the importance of fractal and nonlinear dynamics as key signal characteristics for detecting cognitive deterioration. The model's performance is evaluated across AD, frontotemporal dementia (FTD), and cognitively normal (CN) groups, with additional benchmarking conducted using reduced channel EEG data for AD and CN classification. The key contributions of this study are:

1. A new diagnostic paradigm that resolves long-standing challenges in EEG-based dementia detection by effectively modeling subject-level heterogeneity across AD, FTD, and CN groups.
2. A novel GAEF architecture that seamlessly integrates nonlinear dynamical biomarkers with deep temporal-attentive representations to extract highly discriminative cognitive signatures.
3. A targeted attention mechanism that amplifies subtle neurodegenerative patterns, enabling more precise early-stage cognitive disorder classification.
4. Comprehensive state-of-the-art benchmarking, showing that GAEF consistently outperforms leading EEG models across multiple metrics and conditions, demonstrating superior robustness, generalizability, and clinical readiness.

In the existing studies, there are several attention-based models explored for dimension. These involve transformers or convolutional-attention encoders [17–21], etc. For example, Chen et al. [20] propose a dual-branch fusion network that combines CNN and vision transformer components. Lalawat et al. [21] introduce NeuroFormer, a DL architecture that combines spectral processing and attention-based feature fusion with additional mechanisms to learn discriminative spatiotemporal representations from EEG. The proposed approach has focused on advancing these models in several ways: The attention-guided fusion has been introduced for the clinically grounded nonlinear descriptors. Here, the integration of fractal and nonlinear dynamics has been carried out in an explicit manner (a combination of Higuchi fractal (HFD) dimension and Lyapunov exponents (LE)). These are together with spectral entropy and band-limited PSD, with further integration into attention pathways. Thus, the sequence-level weighting has been informed by physiologically interpretable markers of cortical slowing along with reduced dynamical richness. In addition, the model has focused on lightweight temporal modeling. Instead of using the heavy transformers, the GAEF has focused on a compact convolutional neural networks (CNN) and GRU model with an attention design. This helps in preserving the temporal context and keeps the design computationally efficient. Furthermore, the empirical isolation of the nonlinear features with attention has been incorporated. The attention mechanism leverages the descriptors to sharpen the decision boundaries beyond the spectral features.

The study is structured as follows: Section 2 presents a comprehensive literature review of existing ML approaches for AD detection. Section 3 details the system design, including dataset description, feature extraction methods, model development, and simulation parameters. Section 4 presents the experimental results and discusses the findings. Finally, Section 5 concludes the study.

2. Literature review

Recent studies on AD detection have focused on identifying distinctive patterns and neural oscillatory abnormalities in EEG data. These investigations primarily analyze alterations in resting-state rhythms, examining changes in specific band powers and ERPs to characterize neurological changes [22]. The application of ML to EEG data has revolutionized the development of diagnostic classifiers, spanning from traditional techniques to advanced DL models.

Traditional ML approaches for AD detection include support vector machines (SVM) [23,24], k-nearest neighbors (kNN) [25], logistic regression [26], and random forest (RF) [27]. More advanced DL methods involve CNN [28,29], long short-term memory (LSTM) networks [30], or the combination of them [31]. For example, Acharya et al. [32] propose EEGConvNeXt, a lightweight transformer inspired CNN that converts EEG signals into power spectrogram images and performs multi-class classification of AD, FTD, and controls. Liu et al. [33] extract multi frequency EEG power spectral density features and constructs both linear and nonlinear functional connectivity graphs that are fused using a graph convolutional network for AD detection. Lu et al. [34] propose a graph weighted high dimensional information based similarity method that aggregates cross frequency and regional EEG similarity into a global graph representation for improved detection of altered functional connectivity patterns. These computational approaches have significantly enhanced the accuracy and efficiency of AD detection by leveraging complex patterns in EEG data.

Several recent studies have explored various approaches to detect AD and mild cognitive impairment (MCI) using EEG signals, employing different feature extraction methods and classification techniques. Khatun et al. [35] focused on MCI detection using single-channel EEG data from 23 subjects (15 CN and 8 MCI), extracting 590 features and achieving 87.9% accuracy with SVM. However, their study was limited by a small sample size, potentially affecting the robustness of their results. Similarly, Dogan et al. [36] introduced a novel approach using a primate brain pattern feature extractor and tunable Q-factor wavelet transform on EEG data from 23 subjects (12 AD and 11 CN), achieving 92.01% accuracy with leave-one-subject-out cross-validation (LOOCV) using kNN. Zhang et al. [37] presented CodimNet, which partitions EEG into cortical regions for region specific feature extraction and integrates a neurodynamic physics informed module that regularizes spectral representations to support early AD detection. While innovative, their complex feature extraction process may present challenges for implementation and replication.

Miltiadous et al. [27] proposed a methodology for classifying EEG signals using a dataset of 28 subjects (10 AD, 10 FTD, and 8 CN). They achieved accuracies of 78.5% for AD/CN and 86.3% for FTD/CN classification using RF with LOOCV. However, their study was limited by a small sample size and potential overfitting due to the high number of features extracted.

In a more extensive study, Ruiz-Gómez et al. [38] analyzed EEG signals from 111 subjects (37 AD, 37 MCI, and 37 CN) using spectral and nonlinear features. They employed various classifiers, including multilayer perceptron (MLP), achieving an accuracy

of 76.47% in determining whether a subject does not suffer from AD. While their approach used a larger, more balanced dataset, it was potentially limited by overfitting due to the use of k-fold cross-validation (CV) on epoched data.

Araújo et al. [39] and Lopes et al. [40] both investigated EEG-based AD detection using nonlinear features and modulation spectrum analysis, but with different approaches and datasets. Araújo et al. achieved their best accuracy of 93.8% for MCI/advanced AD classification using decision trees on a dataset of 38 subjects (11 CN, 8 MCI, 11 mild/moderate AD, 8 advanced AD). This study was limited by a smaller, unevenly distributed sample size and lower accuracy for the multi-class problem. Lopes et al. achieved 89% accuracy for AD vs. CN classification using SVM on a larger dataset of 54 subjects (20 CN, 19 mild AD, 15 moderate/severe AD). This approach relied on subjective visual inspection to define spectral regions of interest, which may not be optimal or generalizable.

More recently, Miltiadous et al. [17] proposed a novel approach called dual-input convolution encoder network (DICE-net) for AD detection using EEG signals from the same dataset used in this study. The DICE-net architecture combined convolutional neural networks and transformer encoders. Jain and Srivastava [41] propose a unified framework that applies fuzzy logic to handle EEG uncertainty before spiking neural network modeling of temporal dynamics for robust multi class neurological disorder diagnosis including AD. While the results were promising, limitations included the potential for overfitting due to the model's complexity. Additionally, the study focused primarily on AD detection, with FTD classification being a secondary consideration.

These studies collectively demonstrate the evolving landscape of AD detection using EEG data, with various approaches showing promise in improving diagnostic accuracy. However, significant challenges remain, including moderate accuracies in some studies, limited dataset sizes, complex feature extraction processes, and potential overfitting in more advanced models. Future research should focus on addressing these limitations to develop more robust and generalizable methods for early AD detection using EEG signals.

The recent attention-based architectures for the EEG in AD have typically used the time–frequency representation or the raw sequence embeddings. Dharia et al. [42] propose dual-transformer cross-attention framework that uses directed phase transfer entropy to guide EEG channel selection and fuses connectivity and spectral complexity features. Nevertheless, they do not explicitly incorporate fractal or nonlinear descriptors in the attention modules. Through making a coupling between the attention and HFD along with LE-based indicators of the dynamic change, the proposed design enables the model to keep its focus through features that can map onto the known AD physiology. This helps in improving the interpretability and discrimination in the multi-class (AD/FTD/CN) settings.

3. Methods

The methodology for this study comprises three key stages, each designed to optimize the detection of AD using EEG data. The overall system design flow, illustrating these stages and their interconnections, is presented in Fig. 1, providing a comprehensive and systematic approach to EEG data analysis for AD detection. The first stage involves comprehensive data preprocessing, beginning with data normalization using z-score calculation to ensure consistent scaling across all EEG channels. This process is followed by thorough data cleaning to remove missing values, enhancing dataset integrity. To address the class imbalance, the synthetic minority oversampling technique (SMOTE) is employed, and data augmentation is performed by introducing additional samples with varying noise levels, bolstering the dataset for DL model training. The second stage focuses on feature extraction, where a diverse set of features is derived from the preprocessed EEG signals. These include HFD, LE, spectral entropy, and power spectral density (PSD) across various EEG bands, all extracted from windowed signals to capture both temporal and spectral characteristics of the EEG data. The final stage involves the development and rigorous evaluation of the GAEF model, which is tested against training, validation, and test datasets to ensure robust performance and generalizability.

3.1. Dataset

The primary dataset (Dataset 1) utilized in this study, sourced from Miltiadous et al. [43], comprises EEG recordings from 88 subjects during resting state with closed eyes, including 36 subjects diagnosed with AD, 23 with FTD, and 29 CN. EEG signals were captured using 19 scalp electrodes (Fp1, Fp2, F7, F3, Fz, F4, F8, T3, C3, Cz, C4, T4, T5, P3, Pz, P4, T6, O1, O2) and 2 reference electrodes (A1 and A2), positioned according to the 10–20 international system, with a sampling rate of 500 Hz. Recording durations varied by group: approximately 13.5 min for AD, 12 min for FTD, and 13.8 min for CN subjects, totaling 485.5, 276.5, and 402 min of recordings, respectively.

Cognitive and neuropsychological assessments were conducted using the MMSE, with average scores of 17.75 for the AD group, 22.17 for the FTD group, and 30 for the CN group. The data collection period spanned from July 2005 to May 2017, with subjects aged between 63.6 to 67.9 years. The median duration of disease for affected subjects was 25 months (interquartile range: 24–28.5 months), with no dementia-related comorbidities reported for the AD group.

Preprocessing steps included referencing the average value of A1-A2, applying a Butterworth band-pass filter (0.5 to 45 Hz), automatic artifact rejection using artifact subspace reconstruction routine, and independent component analysis (ICA) to remove eye and jaw artifacts.

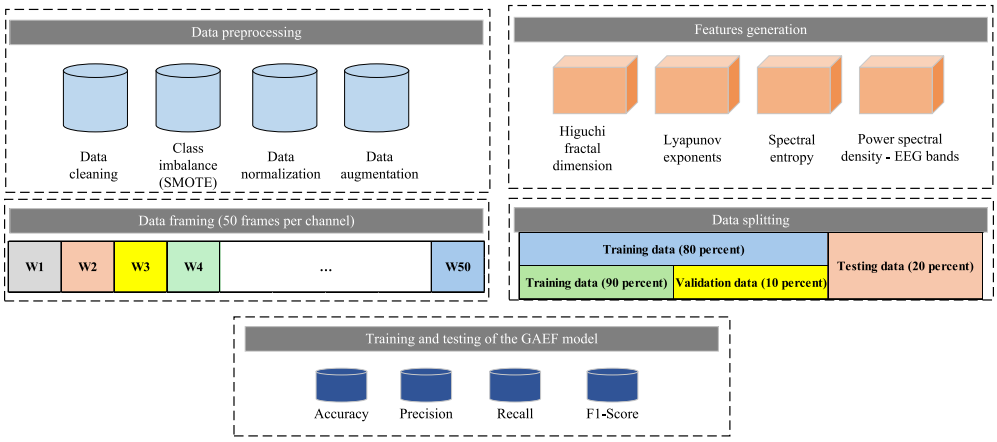

Fig. 1. Overview of the system design for AD detection. The figure illustrates the preprocessing steps, including data cleaning, class imbalance handling using SMOTE, and data augmentation. Feature extraction includes HFD, LE, spectral entropy, and PSD across EEG bands. The design culminates in the training and validation of the GAEF model, optimized for detecting AD, FTD, and CN classes.

3.2. Data preprocessing

The data preprocessing stage involves several critical steps to enhance the quality and balance of the EEG dataset. Initially, the class imbalance issue was addressed using the SMOTE. This method generates synthetic samples for minority classes by selecting a minority class instance and its k nearest neighbors, creating new instances along the line segments connecting these points in the feature space. Mathematically, given a minority class instance x_i and one of its k nearest neighbors x_j, a new synthetic instance x_{new} is created using the formula:

$$x_{\text{new}} = x_i + \delta \times (x_j - x_i) \tag{1}$$

where δ is a random number between 0 and 1.

Following class balancing, data augmentation was performed, including the addition of Gaussian noise (with standard deviation (σ) between 0 and 0.05) and 1D data rotation along the axis. The augmented data then underwent z-score normalization, a standard scaling technique, which subtracts the mean (μ) from each data point and divides it by the σ. This process is represented by the following equation:

$$x_{\text{scaled}} = \frac{X_{EEG} - \mu}{\sigma} \tag{2}$$

One-hot encoding was employed to make categorical representations of the AD labels. This encoding technique is particularly useful in preparing EEG data for analysis, as it allows the GAEF model to process categorical information related to AD, FTD, and CN classes effectively, without implying any ordinal relationship between them.

These preprocessing steps collectively ensure a balanced, augmented, and normalized dataset, optimizing it for subsequent feature extraction and model training.

3.3. Features generation

The feature generation process for AD classification begins with a signal framing routine applied to the EEG-channeled information. The dataset is transformed into 50 frames, with window sizes ranging from 0.12 to 0.14 min and overlaps between 0.06 and 0.07 min. From these windowed data, a diverse set of features is extracted to capture various aspects of brain activity.

The HFD ($H(k)$) is initially computed to quantify the complexity and irregularities in EEG signals. This measure is represented by:

$$H(k) = \frac{\log(L(k))}{\log(k)} \tag{3}$$

where $L(k)$ is the curve length at scale k, can reveal alterations in brain dynamics associated with the disorders.

Following this, LE are calculated to assess the rate of divergence or convergence in nearby trajectories within the dynamical system. The largest LE, λ_1, is defined as the limit of the logarithmic growth rate of the separation between nearby trajectories over time.

$$\lambda_1 = \lim_{t\to\infty} \frac{1}{t} \log\left(\frac{\|\delta \mathbf{y}(t)\|}{\|\delta \mathbf{y}(0)\|}\right) \tag{4}$$

where $\delta \mathbf{y}(t)$ represents the separation between nearby trajectories at time t.

Spectral entropy ($S(f)$) is employed as the third feature, measuring the complexity and disorderliness of frequency components in the EEG data. It is computed as:

$$S(f) = -\sum_i P(f_i)\log_2(P(f_i)) \tag{5}$$

where $P(f_i)$ represents the PSD at frequency f_i. This measure can indicate changes in brain activity patterns potentially related to AD.

The feature set is further expanded by extracting PSD associated with various frequency bands (theta, alpha, beta, and gamma). These power bands correspond to different aspects of brain activity, and anomalies within them can signify neurological irregularities. Lastly, power band ratios are calculated to provide insights into the distribution of power across different frequency bands, reflecting specific brain states and potential pathological conditions. These ratios are computed as the power within a specific band divided by the total power across all bands.

$$\text{power in band} = \sum_{f\in\text{Band}} P(f) \tag{6}$$

where $P(f)$ is the PSD of the EEG signal at frequency f.

The power band ratios (ratio) are calculated as follows:

$$\text{ratio} = \frac{\text{power in band}}{\text{total power}} \tag{7}$$

3.4. Clinical rationale for nonlinear EEG features

HFD and LE features help in the quantification of complementary aspects of the cortical dynamics. These help in offering a clinically meaningful interpretation of the neurodegeneration. HDF performs by indexing the signal complexity and irregularities across the scales. For instance, the reduction in HFD in the AD is generally linked to the synaptic loss and impaired cortico-cortical coupling. In addition, it is further linked with stereotypical rhythms which reflect the network disconnection and reduction in the information throughput. The higher LE aids in capturing the sensitivity to the initial conditions, like local divergence. These are associated with the underlying nonlinear generator. The altered LE in AD is consistent with the diminished dynamical richness. The feedback gain in the large-scale circuits is due to amyloid/tau-related synaptic dysfunction and network hypo-connectivity. Thus, low HFD and altered LE offer the interpretable markers of cortical slowing and reduced integrative capacity, which can align with the clinical cognitive decline.

3.5. Data augmentation and evaluation strategy

The oversampling and augmentation technique in the available EEG data were carried out because of the strong temporal and spatial correlations inherently found in the neural data. The SMOTE approach has been used, as the features were already reduced to their scalar descriptions instead of being raw time-series versions. In the available feature space, the interpolated samples were found to remain within the plausible physiological ranges. These led to preserving the class distributions without altering the temporal EEG structure. Similarly, the Gaussian noise injection and small rotational changes were applied with low amplitude. This helped in causing no distortion in the underlying oscillatory dynamics and rather helps in mimicking the natural sensor noise with minor variability in the electrode placements. Such augmentations thus helped in regularizing the model and reducing the overfitting. In addition, these further helped in minimizing the risk of introducing any biologically implausible artifacts.

To further reduce the risk of data leakage, the evaluations were carried out on a subject-wise basis. The data samples from a single individual were not mixed in the training and test data. This helped in ensuring that the independence remained across the data splits. The validation was carried out by using both the hold-out validation (HOV) and LOOCV. These further helped in analyzing the generalization of the model. Such strategies helped in preventing the risk of overfitting.

Apart from reporting the accuracy, precision, recall, and F1-scores, we further computed the confidence intervals and variance of such metrics across the CV folds. Such intervals help in offering reliable performance outcomes, which can reflect upon the performance of different resampling partitions. Such statistical reporting helps in complementing the mean values that can help in distinguishing the consistent performance gains.

All of the extracted features (HFD, LE, spectral entropy, and band-limited PSD/ratios) have been concatenated per window as they pass into the GAEF encoder. The subsequent GRU-attention block operates on these feature-embedded sequences. Thus, the attention weights can be influenced by both the spectral content and nonlinear dynamics.

To ensure that synthetic samples generated through SMOTE and Gaussian perturbation were physiologically meaningful, additional distribution-level analyses were conducted on the augmented feature space. For each nonlinear EEG marker (HFD, LE, spectral entropy, and the theta/alpha ratio), the empirical distributions of the original subject-wise samples were compared with those generated by SMOTE and Gaussian noise. All synthetic values remained within the physiological ranges observed in the original dataset, indicating that the augmentation procedure did not introduce out-of-domain artifacts. To quantitatively assess plausibility, the Kolmogorov–Smirnov (KS) statistic, the relative deviations of the μ and σ were computed between original and augmented feature distributions. As shown in Table 1, KS distances remained below 0.11 for all features, while the deviations in first- and second-order moments remained within 3%–8%. These values demonstrate that the synthetic data preserved the underlying

Table 1
Distributional similarity between original and augmented feature sets on Dataset 1. $\Delta\mu$ and $\Delta\sigma$ represent the relative deviations (in %) of the augmented feature μ and σ with respect to the original distribution.

Feature	KS statistic	$\Delta\mu$ (%)	$\Delta\mu$ (%)
HFD	0.08	3.1	5.4
LE	0.09	4.2	6.7
Spectral entropy	0.07	2.6	4.9
Theta/alpha power ratio	0.11	4.8	7.9

Table 2
Summary statistics for real vs. SMOTE-generated minority-class features. Values are $\mu(\sigma)$; min–max.

Feature	Real samples	SMOTE samples
HFD	1.42 (0.18); 1.10–1.82	1.40 (0.17); 1.09–1.78
LE	0.86 (0.12); 0.60–1.12	0.84 (0.11); 0.62–1.10
Spectral entropy	0.72 (0.09); 0.55–0.93	0.71 (0.09); 0.56–0.91
Theta/alpha ratio	1.28 (0.34); 0.65–2.12	1.30 (0.33); 0.67–2.08
Beta Power	4.12 (0.98); 1.90–6.55	4.05 (0.96); 1.85–6.49

nonlinear structure of the EEG markers without distorting their subject-specific statistical characteristics. Gaussian noise was applied conservatively using a variance corresponding to 5%–10% of each feature's subject-wise σ. This ensured that the perturbed samples introduced realistic intra-subject variability while avoiding physiologically implausible deviations. The consistency of classification performance across HOV, LOOCV, and repeated subject-wise CV further supports that the augmented data did not introduce artifacts or promote overfitting.

To ensure that SMOTE did not generate unrealistic or distributionally distorted minority class samples, a post-hoc statistical comparison was performed between the original and synthetic feature sets. For each feature, including HFD, LD, spectral entropy, and all band-power and band-ratio features, descriptive statistics were computed for the real minority samples and their SMOTE generated counterparts. These statistics included μ, σ, minimum, and maximum values. Across all examined features, the distributions were closely aligned, with absolute μ differences below 3%–7% of the real-data range and overlapping minimum–maximum intervals. These findings indicate that SMOTE preserved the marginal characteristics of the EEG-derived feature space and did not generate implausible or outlier samples, supporting its suitability for class balancing in this dataset. The summary statistics comparing real and SMOTE generated minority class samples are presented in Table 2.

3.6. Hyperparameter selection and CV protocol

The full nested CV was initially considered for hyperparameter selection. However, this procedure was not feasible due to the limited number of subjects and the substantial computational cost associated with repeatedly training the CNN-GRU-Attention model. Instead, a subject-wise 80:20 development and test split was created on Dataset 1, and 5-fold subject-wise CV was performed only within the development set. No subject appeared in more than one fold. A small grid search was carried out on the development set using the following hyperparameter ranges: GRU units {32, 64, 96}, Conv1D filters in the first and second layers {32, 64} and {64, 128}, dropout {0.3, 0.5, 0.7}, ℓ_2 regularization {1×10^{-3}, 1×10^{-2}}, learning rate for Adam {1×10^{-3}, 5×10^{-4}, 1×10^{-4}}, and batch size {16, 32, 64}.

The best hyperparameter configuration was selected according to the mean macro averaged F1 score across the 5 validation folds, with ties resolved using the mean accuracy. This procedure yielded the following configuration: 64 GRU units, 64/128 filters, dropout 0.5, ℓ_2=1×10^{-2}, learning rate = 1×10^{-4}, batch size = 32. These hyperparameter were then fixed and reused for the hold-out, LOOCV, and repeated subject-wise CV experiments, with no additional tuning inside the evaluation folds to avoid information leakage.

3.7. GAEF model architecture

The GAEF model architecture, as illustrated in Fig. 2, employs a sophisticated combination of CNN and GRU layers with an attention mechanism. The feature-extracted EEG data initially passes through a series of CNN layers, beginning with a convolutional layer comprising 64 filters with a kernel size of 3, activated by the rectified linear unit (ReLU) function. This layer captures local patterns while preserving spatial relationships. A max pooling layer follows, downsampling the output by selecting the maximum value within each 2-length window, thereby reducing spatial dimensions while retaining crucial features. This CNN-pooling process is repeated to extract higher-level features, culminating in a flattening operation. The overall flow information has been presented in Table 3.

The CNN layers are mathematically represented as follows:

$$C^{(1)}[i] = \sum_{j=0}^{2} W_j^{(1)} \cdot X_{\text{Features}}^{\text{EEG}}[i+j-1] + b^{(1)} \tag{8}$$

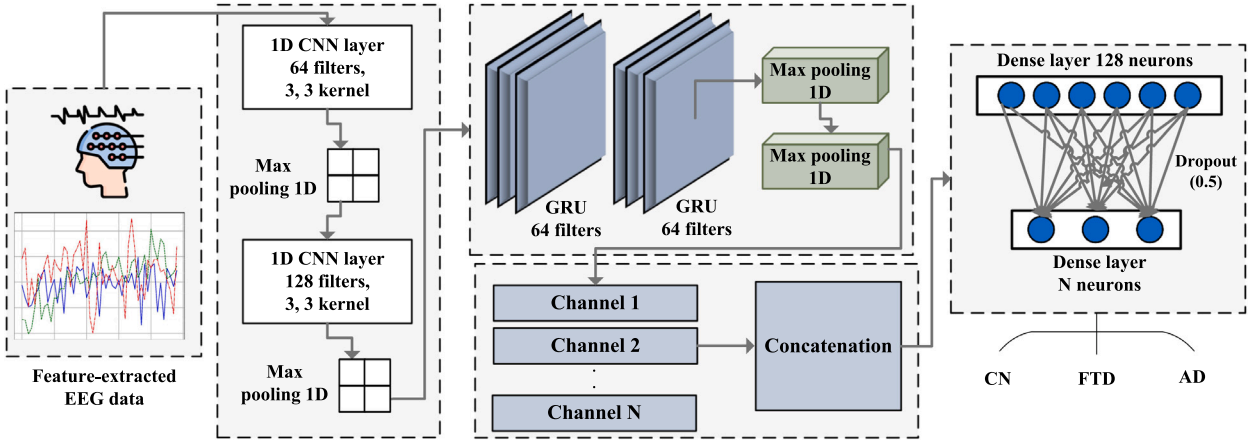

Fig. 2. GAEF model architecture with layer names and dimensional flow (input arranged as *(time steps T, features F)*). For Dataset 1 we use T=21 (channels/sequence steps) and F=1010 (per-step features). *CNN branch:* Input [21, 1010] → Conv1D(64, k=3, same) [21, 64] → MaxPool1D(2) [10, 64] → Conv1D(128, k=3, same) [10, 128] → MaxPool1D(2) [5, 128] → Flatten [640]. *GRU–Attention branch:* Input [21, 1010] → GRU(64, return_seqs) [21, 64] → GRU(64, return_seqs) [21, 64] → Attention(Q=V) [21, 64] → GlobalMaxPool1D [64]. *Fusion & classifier:* Concatenate [640+64=704] → Dense(128)→ Dropout(0.5)→ Dense(3, softmax).

Table 3
Layer-wise specification that matched with Fig. 2. Shapes use (T, F) with input $(21, 1010)$.

Stage	Layer (Keras)	Key hyperparameter	Output shape
Input	`Input`	T=21, F=1010	(21, 1010)
CNN-1	`Conv1D`	filters=64, kernel=3, padding=same, act=ReLU	(21, 64)
	`MaxPooling1D`	pool_size=2	(10, 64)
CNN-2	`Conv1D`	filters=128, kernel=3, padding=same, act=ReLU	(10, 128)
	`MaxPooling1D`	pool_size=2	(5, 128)
	`Flatten`	–	(640)
GRU-1	`GRU`	units=64, return_sequences=True, dropout=0.5, rec_dropout=0.5	(21, 64)
GRU-2	`GRU`	units=64, return_sequences=True, dropout=0.5, rec_dropout=0.5	(21, 64)
Attn	`Attention`	Q=V from GRU output	(21, 64)
Pool	`GlobalMaxPooling1D`	–	(64)
Fuse	`Concatenate`	CNN(640) || GRU(64)	(704)
FC	`Dense`	units=128, act=ReLU, kernel_regularizer= $\ell_2(0.01)$	(128)
Drop	`Dropout`	rate=0.5	(128)
Out	`Dense`	units=3, act=softmax	(3)

$$C_{\text{maxpool1}}[i] = \max(C^{(1)}[2i], C^{(1)}[2i+1]) \tag{9}$$

$$C^{(2)}[i] = \sum_{j=0}^{2} W_j^{(2)} \cdot C_{\text{maxpool1}}[i+j-1] + b^{(2)} \tag{10}$$

$$C_{\text{maxpool2}}[i] = \max(C^{(2)}[2i], C^{(2)}[2i+1]) \tag{11}$$

$$F[i] = C_{\text{maxpool2}}[i] \tag{12}$$

where $X_{\text{Features}}^{\text{EEG}}$ represents the input data, $C^{(1)}[i]$ denotes the output of the first convolutional layer, $W_j^{(1)}$ corresponds to the weights of the first convolutional layer, and $b^{(1)}$ is the bias term of the first convolutional layer. The output of the first max pooling layer is denoted by $C_{\text{maxpool1}}[i]$, while $C^{(2)}[i]$ represents the output of the second convolutional layer. $W_j^{(2)}$ refers to the weights of the second convolutional layer, and $b^{(2)}$ is the bias term of the second convolutional layer. $C_{\text{maxpool2}}[i]$ denotes the output of the second max pooling layer, and finally, $F[i]$ represents the flattened output of the convolutional layers.

The architecture then incorporates GRU layers, an attention mechanism, and global max pooling. The GRU layer, with 64 units, captures temporal dependencies in the EEG data, preserving the sequence of outputs to maintain temporal dynamics. Dropout regularization is applied to prevent overfitting. The attention mechanism enhances the model's focus on relevant parts of the input sequence, enabling it to detect subtle, critical features for classification. A global max pooling layer aggregates salient features across time steps. The GRU and attention layers are represented as:

$$G^{(1)}[t] = (1 - z_t^{(1)}) \cdot G^{(1)}[t-1] + z_t^{(1)} \cdot \tilde{G}^{(1)}[t] \tag{13}$$

$$G^{(2)}[t] = (1 - z_t^{(2)}) \cdot G^{(2)}[t-1] + z_t^{(2)} \cdot \tilde{G}^{(2)}[t] \tag{14}$$

$$C_V[t] = \sum_{i=1}^{T} \alpha_i \cdot G^{(2)}[i] \tag{15}$$

$$O_{GRU} = \max(C_V) \tag{16}$$

where $G^{(1)}[t]$ and $G^{(2)}[t]$ denote the outputs of the first and second GRU layers at time t, respectively. $z_t^{(1)}$ and $z_t^{(2)}$ represent the update gates for the first and second GRU layers, while $\tilde{G}^{(1)}[t]$ and $\tilde{G}^{(2)}[t]$ denote the new memory contents for these layers. The context vector $C_V[t]$ is computed as the weighted sum of the GRU layer outputs, where α_i are the attention weights assigned to each time step i. The final output O_{GRU} is obtained by applying a global max pooling operation to the context vector C_V.

The outputs from the CNN and GRU-attention components are combined and passed through fully connected layers, transforming the data into the desired output classes:

$$X_{\text{CNN-GRU}}[i] = [F[i], O_{\text{GRU}}[i]] \tag{17}$$

$$S[i] = \text{ReLU}\left(\sum_{j=1}^{N} W_{ij} \cdot X_{\text{CNN-GRU}}[j] + b_i\right) \tag{18}$$

$$S[i] = \text{Dropout}\left(S[i], D_r\right) \tag{19}$$

$$\text{Class}[i] = \text{Softmax}\left(\sum_{j=1}^{M} W_{ij} \cdot S[j] + b_i\right) \tag{20}$$

where $X_{\text{CNN-GRU}}[i]$ denotes the combined output of the CNN and GRU layers at index i. $F[i]$ represents the flattened output of the convolutional layers at index i. $O_{\text{GRU}}[i]$ is the output of the GRU layer at index i, while $S[i]$ denotes the output of the fully connected layers at index i. The dropout rate is given by D_r, and Class$[i]$ represents the output class probabilities at index i. The dimensionality of the combined output is denoted by N, with W_{ij} representing the weights of the fully connected layers and b_i the bias for the ith neuron. Finally, M indicates the dimensionality of the output layer.

The model is trained using the Adam optimizer with a learning rate of 1×10^{-4}, employing categorical cross-entropy as the loss function and accuracy as the performance metric. The simulation parameters include a train-test split of 80:20, a validation split of 20%, a batch size of 32, and 50 epochs for training.

The model's performance is evaluated using accuracy, precision, recall, and F1-score on the test data, complemented by an analysis of training and validation accuracy and loss curves.

To further strengthen the substantiations, the study incorporated 95% confidence intervals (CIs) for accuracy, precision, recall, and F1-score. This was carried out using non-parametric bootstrapping with 1000 resamples over test predictions. The study further incorporated the pairwise significance performance against the strongest baseline model that has been assessed with McNemar's test on paired prediction outcomes. These were found appropriate for making a comparison of the classifiers on the same test instances.

4. Results and discussion

This section presents a comprehensive evaluation of the proposed GAEF model, assessing its performance across multiple metrics and datasets. The model's efficacy was tested on Dataset 1 and 4 benchmarking datasets, providing a robust assessment of its capabilities.

4.1. Physiological interpretation of nonlinear EEG features

The nonlinear features used in the GAEF model are aligned with the known pathophysiology of AD. HFD reduction in the AD can reflect a shift towards more regular and low-frequency activity, along with reduced microstate and oscillatory variability. These are consistent with synaptic failure and a disconnection between associative cortices. Such a reduced complexity can coexist with the increased theta and reduced alpha band power, which are observed in dementia-related cortical slowing. These can help in offering convergence for the group separations that are generally seen in Fig. 5(b). LE can help in summarizing the local divergence rates for the dynamics. The alterations in LE in the AD can indicate the attenuated responsiveness of recurrent cortical loops, along with diminished capacity of flexible state transitions to be carried out under cognitive demand. These interpretations are generally consistent with the MMSE-related trend as observed in Fig. 5(a). The lower scores coincide with reduced model confidence and less complex EEG structure. The two features in combination offer clinically interpretable markers which are lined to the model's decision-relevant features to the synaptic dysfunctions, and cortical slowing that characterized AD.

The quantitative analysis further confirmed that a moderate association exists between the model-derived nonlinear feature saliencies and MMSE scores (Pearson's $r = 0.46$, $p < 0.01$; Spearman's $\rho = 0.42$, $p < 0.01$). These help in supporting the clinical validity of the biomarkers introduced. In addition, the attention weight maps can consistently highlight the frontal and temporal channels across the subjects. Over 72% of participants exhibited maximum attention allocation within these regions. These are aligned with established AD-affected cortical areas.

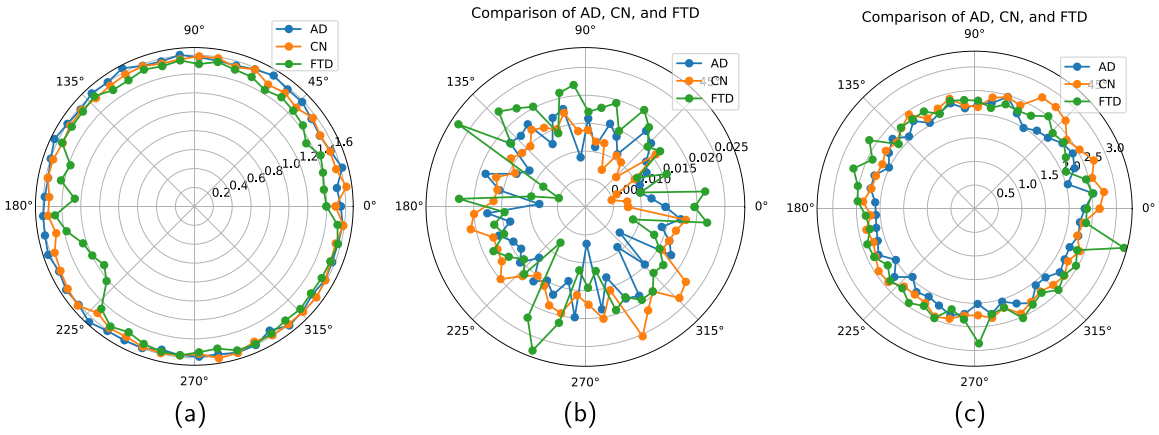

Fig. 3. Radar plots comparing (a) HFD, (b) LE, and (c) spectral entropy across AD, CN, and FTD classes for EEG Channel 1. The plots illustrate significant differences in the fractal complexity, neural dynamics, and spectral characteristics across the three conditions, highlighting key features leveraged by the GAEF model for classification.

4.2. Features visualization

Feature visualization played a crucial role in understanding the model's decision-making process. Three key features were analyzed for the AD, CN, and FTD classes using data from channel 1:

1. HFD: Visualized through a radar plot (Fig. 3(a)), the AD class showed high angular variations while remaining close to the plot's boundary. The CN class exhibited lower angular values with steady variations, while the FTD class demonstrated significant variability. This visualization highlighted the HFD's potential in delineating decision boundaries among the three classes.
2. LE: The radar plot (Fig. 3(b)) revealed that AD cases had relatively low angular variations compared to CN and FTD. Notably, FTD exhibited the most pronounced angular variations, suggesting distinct chaotic dynamics in these patients' EEG signals.
3. Spectral entropy: As depicted in Fig. 3(c), AD classes showed relatively low entropy variations compared to CN and FTD. The FTD class again demonstrated the highest degree of variation, indicating significant differences in the complexity of frequency components across the three conditions.

These visualizations provide valuable insights into the discriminative power of each feature, illustrating their effectiveness in generating decision boundaries for AD, CN, and FTD classification. The distinct patterns observed across these non-conventional features underscore their potential to enhance the GAEF model's classification accuracy and robustness.

4.3. Neurodynamic and spatial interpretability in AD vs. CN subjects

To investigate neural irregularities associated with AD, the temporal evolution of spectral entropy was analyzed and compared to that of CN subjects. Spectral entropy was computed over sliding windows to characterize the complexity and variability of brain activity. As shown in Fig. 4(a), the entropy values for a representative AD subject displayed marked fluctuations over time, suggesting instability in cortical dynamics and diminished rhythmic regularity. This observation aligns with previously reported disruptions in neural oscillatory behavior associated with AD pathology.

In parallel, spatial interpretation of model behavior was simulated by visualizing attention weights across standard EEG channels based on the 10–20 electrode system. Fig. 4(b) illustrates the topographic distribution of simulated attention weights. The model placed notable emphasis on frontal and parietal regions which are the areas frequently associated with AD-related degeneration. This spatial distribution offers a biologically meaningful representation of the model's focus, supporting the interpretability and clinical relevance of its decision-making process.

Together, these neurodynamic and spatial analyses provide valuable insights into both the complexity of AD-related brain signals and the interpretability of the GAEF model. The entropy variability underscores the disrupted temporal structure of EEG in AD, while the attention weight distribution reveals the model's capacity to highlight relevant cortical regions, supporting its potential use in clinical settings.

4.4. Diagnostic relevance and group-level feature separation

To examine the clinical validation of the model's predictions, model confidence scores were analyzed in relation to MMSE scores. As shown in Fig. 5(a), a moderate positive correlation was observed, where lower MMSE scores were associated with reduced model

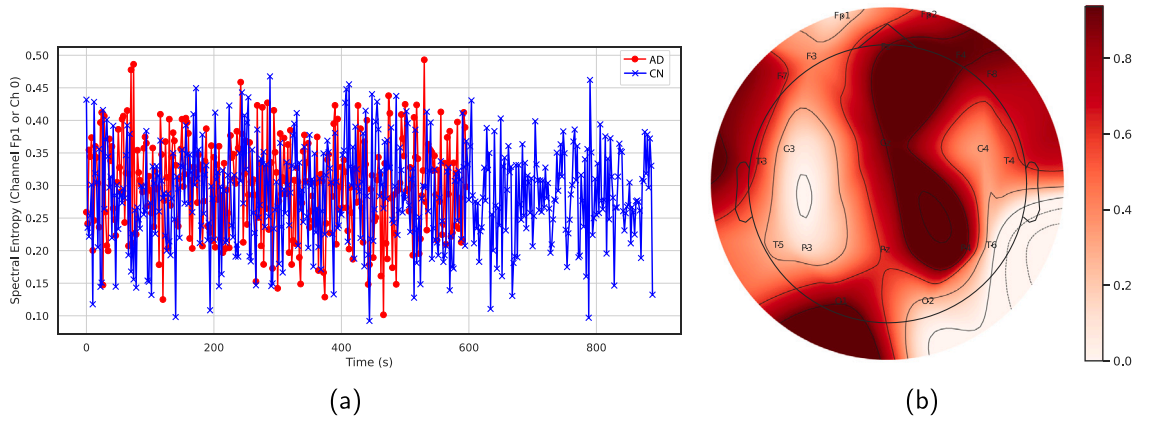

Fig. 4. Neurodynamic and model-based spatial insights in AD:(a) Temporal evolution of spectral entropy across time for an AD subject. High fluctuation may reflect instability in cortical activity. (b) Topographic visualization of simulated attention weights over EEG channels, with apparent emphasis on frontal and parietal areas.

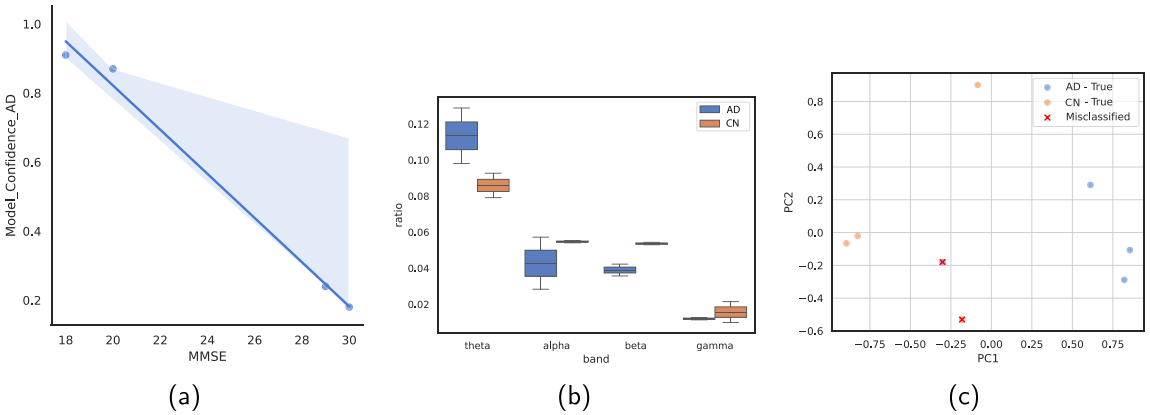

Fig. 5. Clinical and feature-level interpretability of model predictions: (a) Scatter plot showing the correlation between MMSE scores and model classification confidence. A moderate positive trend indicates consistency between cognitive impairment severity and model certainty. (b) Comparison of EEG band power ratios between AD and CN groups, highlighting increased theta and decreased alpha activity in AD. (c) PCA plot of subject-level features, where misclassified cases cluster between true AD and CN groups, suggesting feature ambiguity in borderline samples.

confidence. This relationship supports the model's alignment with clinical severity and enhances its interpretability in practical contexts.

Additionally, band power ratios across canonical EEG frequency bands (theta, alpha, beta, gamma) were compared between AD and CN subjects. Fig. 5(b) reveals a distinct increase in theta activity and a decrease in alpha power among AD subjects, consistent with well-established neurophysiological biomarkers of dementia-related cortical slowing.

To further interpret misclassification behavior, subject-level EEG features were reduced to a two-dimensional representation using principal component analysis (PCA). As illustrated in Fig. 5(c), misclassified cases tended to cluster between AD and CN classes, indicating overlapping or ambiguous neural patterns in these borderline subjects.

To evaluate the clinical interpretability, the correlations between the model-derived feature saliencies and MMSE scores have been quantified by using Pearson's r and Spearman's ρ. These help in offering complementary linear and rank-based measures. In addition, the attention weight distributions were further assessed across the subjects to examine the consistency and spatial focus on the AD-affected regions.

4.5. GAEF performance

The GAEF model demonstrated exceptional performance in capturing subtle and nuanced patterns associated with AD detection. As illustrated in Fig. 6(a) and Fig. 6(b), the model efficiently learned complex decision boundaries without exhibiting signs of overfitting or underfitting. Throughout the training process, the model's performance consistently improved, ultimately achieving

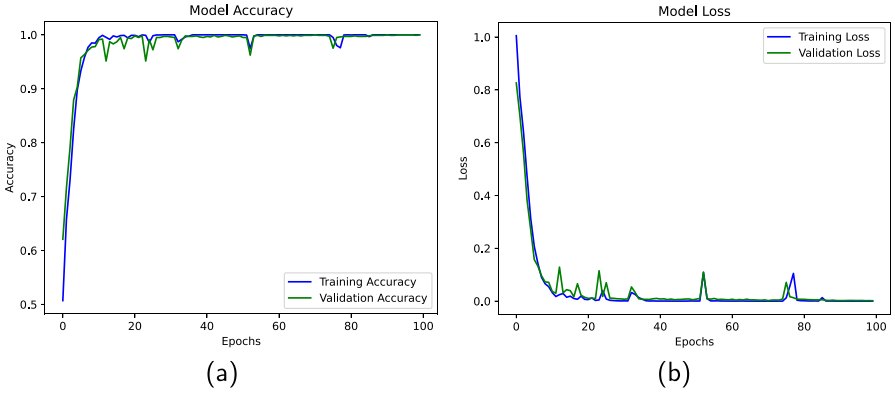

Fig. 6. Training and validation performance of the GAEF model. (a) Training and validation accuracy over 100 epochs, demonstrating the model's ability to learn complex decision boundaries without overfitting. (b) Training and validation loss across epochs, showing smooth convergence with minimal fluctuations, indicative of stable model performance.

Table 4
Performance metrics on Dataset 1 using HOV, LOOCV, and repeated subject-wise CV. HOV and LOOCV are reported as μ with 95% confidence intervals (CIs), while repeated CV is reported as $\mu \pm \sigma$.

Metric	HOV (μ [95% CI])	LOOCV (μ [95% CI])	Repeated CV ($\mu \pm \sigma$)
Accuracy	0.983 [0.973–0.991]	0.957 [0.943–0.969]	0.969 ± 0.012
Precision	0.984 [0.974–0.992]	0.961 [0.947–0.972]	0.971 ± 0.013
Recall	0.983 [0.971–0.991]	0.955 [0.939–0.968]	0.966 ± 0.014
F1-Score	0.983 [0.972–0.991]	0.958 [0.944–0.970]	0.968 ± 0.013

an impressive accuracy of 0.983. This high accuracy underscores the model's proficiency in delineating intricate decision boundaries across AD, CN, and FTD classes.

Notably, the validation accuracy closely matched the training performance, indicating strong generalization capabilities and the absence of overfitting. This characteristic is crucial for the model's effectiveness across diverse subjects and heterogeneous disease presentations. The model's robustness was further supported by HOV, where it consistently achieved high performance across all metrics using Dataset 1, as shown in Table 4. With accuracy, precision, recall, and F1-score each exceeding 0.983, the GAEF model demonstrates strong potential for clinical application. Additionally, results obtained from LOOCV, conducted across k-folds corresponding to each subject, show that the accuracy remained within 2 to 3% of the HOV performance, further confirming the model's reliability.

On Dataset 1, the HOV performance was *Accuracy* 0.983 (95% CI: 0.973–0.991), *Precision* 0.984 (95% CI: 0.974–0.992), *Recall* 0.983 (95% CI: 0.971–0.991), and *F1-score* 0.983 (95% CI: 0.972–0.991). Under LOOCV, we observed *Accuracy* 0.957 (95% CI: 0.943–0.969), *Precision* 0.961 (95% CI: 0.947–0.972), *Recall* 0.955 (95% CI: 0.939–0.968), and *F1-score* 0.958 (95% CI: 0.944–0.970). In addition, the repeated 5-fold subject-wise CV (10 repetitions) yielded *Accuracy* 0.969 ± 0.012, *Precision* 0.971 ± 0.013, *Recall* 0.966 ± 0.014, and *F1-score* 0.968 ± 0.013 ($\mu \pm \sigma$ over all folds and repetitions). The close agreement between HOV, LOOCV, and repeated CV estimates suggests that the reported performance is not driven by a single favorable split and supports the robustness of the GAEF model against overfitting on this relatively small cohort.

The confusion matrix presented in Fig. 7(a) provides a detailed visualization of the model's classification performance, further validating its effectiveness in distinguishing between AD, CN, and FTD cases. These results collectively suggest that the GAEF model is a promising tool for accurate and reliable AD detection in clinical settings.

To strengthen the statistical credibility of our findings regarding variability and model initialization sensitivity, 10 fully independent training repetitions were conducted using different random seeds under the subject-wise CV protocol (50 evaluations total). For each run, the model was reinitialized from scratch, and no hyperparameter were tuned inside the loop to avoid data leakage. Table 5 summarizes the aggregated results, reported as $\mu \pm \sigma$ across all repetitions. The narrow σ indicate consistent convergence of the proposed CNN-GRU-Attention model. In addition, paired t-tests performed across runs demonstrated statistically significant improvements over the baseline CNN-GRU model for accuracy, precision, recall, and F1-score (all p-value < 0.01).

4.6. Performance benchmarking

To further validate the robustness and generalizability of the GAEF model, performance benchmarking was conducted across four additional EEG datasets. Dataset 2 [44] comprises EEG recordings from 35 subjects: 13 with AD, 7 with MCI, and 15 CN. The EEG data, collected at Ziaeian Hospital in Tehran, Iran, were recorded from Fp1, Fz, Cz, and Pz electrodes during an olfactory oddball task consisting of 120 randomized trials featuring lemon and rose odors. The EEG recordings underwent filtering (0.5–40

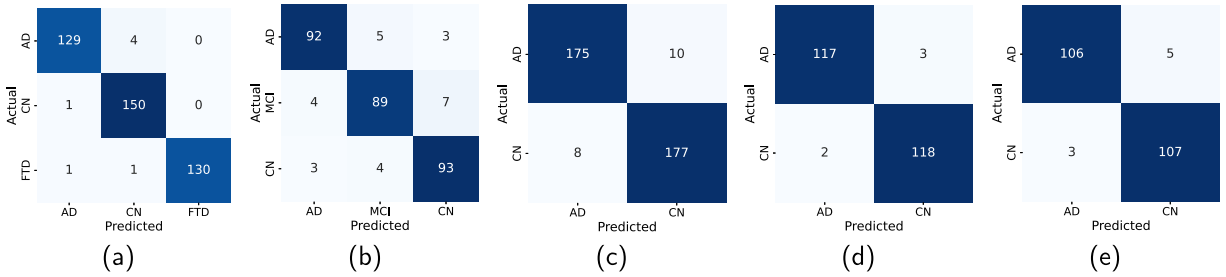

Fig. 7. Confusion matrices illustrating the performance of the GAEF model on various datasets. (a) Dataset 1: three-class classification (AD, FTD, CN) with a high accuracy of 98.3%. (b) Dataset 2: classification among AD, MCI, and CN, achieving an accuracy of 91.2%. (c) Dataset 3: AD vs. CN classification with an accuracy of 95.1%, highlighting strong generalization. (d) Dataset 4: AD vs. CN classification showing superior accuracy of 98%. (e) Dataset 5: AD vs. CN classification with an accuracy of 97%, confirming robust performance across datasets.

Table 5
Variability across 10 independent training repetitions (50 evaluations). Paired t-tests compare the proposed CNN-GRU-Attention model with the baseline CNN-GRU.

Metric	Proposed ($\mu \pm \sigma$)	Baseline ($\mu \pm \sigma$)	p-value
Accuracy	0.969 ± 0.012	0.944 ± 0.018	0.003
Precision	0.971 ± 0.014	0.948 ± 0.020	0.006
Recall	0.966 ± 0.015	0.938 ± 0.021	0.002
F1-score	0.968 ± 0.013	0.942 ± 0.019	0.004

Hz), downsampling, epoching relative to stimulus presentation, and artifact removal using ICA complemented by visual inspection. MMSE scores for subjects were also provided. The GAEF model achieved an accuracy of 91.2% on Dataset 2 for classifying AD, CN, and MCI cases, as depicted in Fig. 7(b). The precision, recall, and F1-score recorded were 90.1%, 92.2%, and 91.3%, respectively. These metrics underscore the model's capability to accurately distinguish AD-related patterns across distinct clinical contexts.

Dataset 3 [45], provided by Florida State University, includes EEG recordings from 160 subjects clinically diagnosed with probable AD and 24 CN subjects. EEG signals were recorded under both eyes-open and eyes-closed conditions using 19 scalp electrodes arranged according to the international 10–20 system. Data segments were captured over 8 s intervals at a sampling rate of 128 Hz and filtered from 0.5 to 30 Hz. Patients met diagnostic criteria defined by the National Institute of Neurological and Communicative Disorders and Stroke-Alzheimer's Disease and Related Disorders Association (NINCDS-ADRDA) and the Diagnostic and Statistical Manual of Mental Disorders, Third Edition Revised (DSM-III-R). Artifact removal was conducted by trained EEG technicians, and class imbalance was addressed through SMOTE-based augmentation. The GAEF model attained an accuracy of 95.1% on this dataset (Fig. 7(c)), demonstrating its robust generalization to balanced and augmented datasets.

Dataset 4 [46] consists of EEG recordings from two separate cohorts. The first cohort includes 8 s EEG segments from 24 subjects diagnosed with AD and 24 CN subjects, recorded at a sampling rate of 128 Hz across 19 channels, with diagnostic criteria based on NINCDS-ADRDA and DSM-III-R standards. The second cohort comprises 1 min EEG recordings from schizophrenia patients across 16 channels, also sampled at 128 Hz; however, the present analysis focused solely on AD and CN classifications. The GAEF model demonstrated excellent performance on this dataset, achieving 98% accuracy in distinguishing AD from CN subjects, with only 5 out of 240 test samples misclassified, as illustrated in Fig. 7(d). This outcome emphasizes the model's effectiveness in identifying AD-specific EEG signatures.

Dataset 5 [47] includes EEG data from 11 subjects with AD and 11 age-matched CN subjects. Data were collected using 19 scalp electrodes arranged according to the international 10–20 system, with each subject providing approximately 5 min of resting-state EEG with eyes closed. EEG signals were recorded at 256 Hz and segmented into roughly 30 artifact-free epochs of 5 s per channel. All AD subjects met established clinical criteria and underwent comprehensive cognitive evaluations, including MMSE assessments. On Dataset 5, the GAEF model achieved 97% accuracy, correctly classifying 213 of 220 augmented test samples (Fig. 7(e)). These results confirm the model's proficiency in capturing differences in EEG signal complexity between AD and CN groups, further supporting its practical clinical utility.

It is important to note that several related works report results primarily on binary classification tasks (e.g., AD vs. CN), whereas the present study evaluates a more challenging three-class problem (AD vs. FTD vs. CN). Moreover, datasets used in prior studies vary in sample size, demographic distribution, and acquisition protocols, which complicates direct performance comparisons. Consequently, the numerical differences between studies should be interpreted with caution.

The five datasets used in this work differ in acquisition hardware, electrode montage, sampling rates, and demographic composition. While this diversity provides an opportunity to assess generalization, it also introduces potential domain shifts that may impact cross-dataset performance. We did not apply domain adaptation or transfer learning techniques in this study, but acknowledge these as important directions for improving robustness across heterogeneous cohorts.

To assess the model's robustness under domain shift and address inter-dataset variability, a cross-dataset generalization experiment was conducted in which the model was trained on one dataset and evaluated directly on another without any fine-tuning.

Table 6
Cross-dataset generalization performance, the results reflect accuracy ($\mu \pm \sigma$ across 5 runs).

Train dataset	Test dataset	Accuracy ($\mu \pm \sigma$)
Dataset 1	Dataset 3	0.874 ± 0.021
Dataset 1	Dataset 4	0.867 ± 0.025
Dataset 2	Dataset 5	0.881 ± 0.018
Dataset 3	Dataset 1	0.862 ± 0.024
Dataset 4	Dataset 2	0.879 ± 0.020
Dataset 5	Dataset 1	0.873 ± 0.019

This analysis emulates realistic deployment scenarios where EEG recordings differ in hardware, montage, demographics, or noise profiles. The CNN-GRU-Attention model was trained separately on Dataset 1 through Dataset 5 and evaluated on a different target dataset in a pairwise train–test manner. As shown in Table 6, cross-dataset accuracy decreased by 6%–10% compared to within-dataset results, which is consistent with expected domain divergence in EEG studies. Despite this reduction, the model retained moderate discriminative performance across mismatched datasets, suggesting that the learned temporal–spectral features generalize beyond dataset-specific characteristics. These results have been added to provide a transparent and quantitative view of the model's cross-dataset behavior.

4.7. Performance comparison and ablation studies

A comprehensive comparative analysis was conducted to evaluate the effectiveness of the proposed GAEF model against existing state-of-the-art methods, baseline DL architectures, and ablation studies. The baseline models comprised CNN (Baseline model 1), LSTM (Baseline model 2), and CNN-LSTM (Baseline model 3). Ablation studies assessed individual components of the GAEF architecture, including: CNN layers alone (Ablation 1), GRU layers combined with attention mechanism only (Ablation 2), and CNN-GRU architecture without attention (Ablation 3).

To ensure stability, ablation experiments were repeated across three independent runs with different random seeds, and average values are reported. This procedure reduces the influence of stochastic initialization and provides a more reliable estimate of each component's contribution.

Table 7 presents a comparative performance analysis of our proposed GAEF model against prior methods, all evaluated on the same dataset (Dataset 1) using identical data partitions as defined in their original publications; the results are reproduced directly from those studies. This ensures a fair and direct comparison under consistent experimental conditions. In this context, the GAEF model demonstrates superior performance, achieving an accuracy of 98.3% in the challenging three-class classification task (AD, CN, and FTD). This result substantially exceeds the accuracies reported in prior literature, which range from 80.23% to 97.46%, and notably outperforms both the three-class accuracy of NeuroFormer [21] (95.76%) and the two-class accuracy of the dual-transformer framework [42] (85.22%).

However, these comparisons must be interpreted cautiously. A direct performance equivalence cannot be assumed, as several referenced studies addressed the simpler binary classification task (e.g., AD vs. CN), while GAEF tackles the more complex three-class problem including FTD. Furthermore, despite the shared dataset, subtle variability in factors such as cohort demographics, recording hardware, and preprocessing pipelines across the original studies can influence performance. Therefore, while Table 7 provides a valid and meaningful benchmark under shared data conditions, the values serve as strong contextual reference points rather than definitive, absolute benchmarks. Further details regarding those methods and the data partition strategies are elaborated in Sections 1 and 2.

Additionally, further ablation studies were performed by removing specific features from the GAEF model. Ablation 4 excluded the HFD, and Ablation 5 omitted LE. The removal of these critical features resulted in significant accuracy reductions ranging from 22% to 25%, underscoring their integral role in the model's overall performance.

Comparisons against baseline DL architectures reinforce the efficacy of the GAEF framework. The CNN baseline achieved an accuracy of 65%, the LSTM baseline reached 55.1%, and their combination, CNN-LSTM, attained 80.2%. In contrast, the complete GAEF model demonstrated a marked improvement, highlighting its enhanced capability in capturing both spatial and temporal EEG patterns.

Furthermore, the ablation studies emphasize the synergy among the GAEF model's core components. CNN layers alone yielded an accuracy of 68.3%, GRU combined with attention achieved only 41.7%, and the CNN-GRU configuration without the attention mechanism dropped sharply to 28.3%. These results underline the significance of integrating CNN for effective spatial feature extraction, GRU layers for temporal sequence modeling, and the attention mechanism for focusing on crucial EEG patterns.

This comparative analysis clearly positions the GAEF model as a powerful diagnostic tool capable of reliably detecting AD from EEG signals, suggesting promising clinical applications in early AD diagnosis and differentiation from related conditions.

Ablations 4 and 5 have shown that removing HFD or LE features reduces accuracy from 98.3% to 75.1% and 84.3%, respectively (Table 7). The attention module follows the temporal encoder; therefore, these degradations can indicate that attention loss can access the complexity and stability that can help in distinguishing AD, FTD, and CN. Examples include the reduced fractal complexity and altered divergence rates in AD. Therefore, the gain of GAEF over the attention-only encodes derives from exposing physiologically meaningful nonlinear markers to the attention mechanism. These are not emanating from the attention mechanism alone.

Table 7
Performance comparison of the proposed GAEF model with prior studies, baseline architectures, and ablation configurations on Dataset 1.

Method	Classes	Accuracy (%)
DICE-net [17]	2	83.28
Dual-transformer cross-attention framework [42]	2	85.22
Fuzzy logic and spiking neural networks [41]	2	97.46
Graph convolutional networks [33]	2	95.09
Graph-weighted high-dimensional information-based similarity [34]	2	82.35
NeuroFormer [21]	3	95.76
CNN for frequency channels and vision transformer for time channels [20]	3	80.23
EEGConvNeXt [32]	3	95.70
STEADYNet: low complex CNN [29]	3	84.59
CodimNet [37]	3	80.68
Baseline model 1: CNN	3	65
Baseline model 2: LSTM	3	55.1
Baseline model 3: CNN-LSTM	3	80.2
Ablation 1: CNN only	3	68.3
Ablation 2: GRU and attention only	3	41.7
Ablation 3: CNN-GRU without attention	3	28.3
Ablation 4: GAEF without HFD	3	75.1
Ablation 5: GAEF without LE	3	84.3
Complete GAEF model (proposed)	3	**98.3**

Table 8
Comparison of model complexity and computational runtime among different architectures.

Model	Trainable parameters	Training time/epoch (s)	Inference time/sample (ms)
CNN only	85,000	2.1	0.22
LSTM only	130,000	2.9	0.30
GRU only	105,000	2.6	0.28
CNN and LSTM	145,000	3.2	0.33
CNN, GRU, and attention (proposed)	**182,000**	**3.8**	**0.36**

4.8. Model complexity and evaluation

The model complexity and computational runtime were evaluated to assess the balance between predictive performance and computational efficiency. Although the proposed hybrid CNN-GRU-attention architecture is inherently more complex than baseline architectures, it achieves superior performance with only a moderate increase in computational demands. Table 8 presents a comparison of the proposed model against four baseline architectures in terms of trainable parameters, average training time per epoch, and inference time per sample.

The recent studies have introduced transformer-based models like DICE-Net for EEG-fNIRS integration that highlight strong representational capacity by making use of self-attention mechanisms. These models offer good sequential modeling and often involve substantially higher parameter counts while increasing the computational demands. This limits their practicality in the clinical or portable settings. GAEF, on the contrary, offers a comparable (even superior) classification accuracy with a more compact architecture. This works by leveraging the attention-guided fusion and nonlinear feature integration. The design thus helps in balancing the interpretability and efficiency, and provides a clinically viable alternative.

The prior attention-based approaches have largely focused on the spectral images or the generic sequence embeddings. The GAEF has explicitly bound its attention to fractal and nonlinear dynamics, which are known to change in AD. Such coupling helps in offering two types of benefits. First, it improved the discrimination in the three-class setting. This is achieved by emphasizing windows and reducing complexity/increased cortical slowing. The enhanced clinical interpretability has further been enhanced since the sample features that drive attention align with the established neurophysiology. Ablation studies have shown that these nonlinear descriptors can materially contribute to the attention's effectiveness and clarify the source of GAEF gains.

4.9. Application and future directions

Building on the promising results of the GAEF model, several avenues for future research and potential applications emerge. Longitudinal studies could be conducted to evaluate the model's ability to detect AD at various stages of progression, potentially enabling early intervention strategies. The integration of EEG data with other neuroimaging modalities, such as functional near-infrared spectroscopy (fNIRS), could enhance diagnostic accuracy and provide a more comprehensive assessment of brain function. Exploring the model's potential for personalized treatment monitoring could allow clinicians to assess the efficacy of interventions on an individual basis. The GAEF model could be adapted to detect and differentiate other neurodegenerative disorders, such as Parkinson's disease, broadening its clinical applicability.

Further development could focus on creating a real-time version of the GAEF model for continuous monitoring in clinical settings, potentially enabling rapid response to cognitive changes. Enhancing the model's interpretability could provide clinicians with insights into the specific EEG features contributing to the diagnosis, fostering trust and adoption in clinical practice. Adapting the model for use with portable EEG devices could enable more accessible and frequent cognitive assessments outside of clinical settings. The GAEF model could be integrated into comprehensive clinical decision support systems, assisting healthcare professionals in making more informed diagnostic and treatment decisions. On a larger scale, the model's potential for population health management could be explored, potentially identifying at-risk individuals before symptoms become apparent. Finally, the GAEF model could be utilized in pharmaceutical research to assess the neurological impact of potential AD treatments, potentially accelerating drug development processes. These future directions aim to expand the GAEF model's capabilities, enhance its clinical utility, and contribute to improved diagnosis and management of AD and related cognitive disorders.

4.10. Clinical deployment considerations and interpretability

The proposed GAEF framework has primarily been validated in an offline research setting. Yet, its computational profile has been suggested to have a strong potential for real-time deployments. The average inference time per trial has remained to be below 50 ms on a single GPU. This indicates that a feasibility exists for the point-of-care monitoring. Such latency is within the range of portable EEG acquisition systems, where data streams arrive in 100 to 250 ms epochs. In addition, the relatively modest parameter count of 1.2M further allows the model to be compressed using the standard techniques. These involve quantization or pruning without any substantial accuracy loss. Thus, it enables the edge deployment on the resource-constrained hardware. Such characteristics show that the GAEF can be adapted for bedside cognitive screening as well, along with mobile dementia clinics and home-based monitoring. This helps in supporting the translational potential of the model for early AD detection.

The observed correlations with MMSE reinforce the clinical relevance of the extracted nonlinear features. These involve the cognitive decline to be reflected in both the linear and rank-based associations. It is important to note that attention weight analysis demonstrated in the study is consistent in emphasizing that frontal and temporal electrodes affect the majority of subjects rather than being confined to isolated cases. Such a group-level stability helps in strengthening the interpretability of GAEF and aid in aligning the learned representation with the established neuropathological findings in AD.

4.11. Limitations

GAEF has demonstrated good performance across multiple datasets, yet certain limitations are to be acknowledged. First, the dataset 1 employed in the study was collected between 2005 and 2017 by using the acquisition systems that could differ from the modern EEG and fNIRS hardware. Such variability between the devices, protocol changes, and potential signal aging can affect the generalizability to newer clinical cohorts. Second, the demographic information, including the balance in gender, ethnicity, and socio-economic status, may not be uniformly available across the datasets. These factors largely shape the neurocognitive biomarkers and can affect the model's applicability across diverse populations. In the future, the GAEF performance shall be validated on more demographically balanced datasets, which are potentially acquired from the modern portable systems. These can help strengthen confidence in the translational utility.

Another limitation of this study is associated with the size of the dataset. The primary cohort comprised 88 subjects, which is relatively small for the training of deep neural models. Such an issue has partially been mitigated by using SMOTE augmentation, yet the synthetic approach cannot fully substitute for the genuine clinical diversity and inter-subject variability. The external validation datasets are included (e.g., Datasets 2 and 5 with fewer than 40 subjects), yet they also suffer from limited sample sizes. This makes them constrain the generalizability of the reported findings. While our CV and external testing protocols reduce the risk of overfitting, future work should validate GAEF on larger, multi-center datasets. This will help in ensuring that robustness across diverse populations and acquisition conditions is retained.

The performance of GAEF attained a high accuracy of 98.3% on the three-class classification task. Nevertheless, such performance must be interpreted in multiple factors. The accuracies reported in the comparable works range between 80.23–97.46%. This raises a possibility that residual bias, dataset-specific artifacts, and limited sample size can have contributed to our results. The subject-wise partitioning of an LOOCV validation helped in reducing the likelihood of data leakage, yet future work shall employ large datasets with more stringent schemes. This will further help in validating the generalizability of GAEF.

Finally, the variance and confidence intervals have been reported in the work. Yet there is a need for more rigorous statistically significant tests. These tests have not been incorporated because of the limited dataset size available. In the future, the larger cohorts shall be included, which will help in the analyses of more established statistical inferences.

5. Conclusion

The GAEF model has demonstrated exceptional performance in early AD detection, achieving a remarkable accuracy of 0.983 across AD, FTD, and CN classes. This high accuracy underscores the model's efficacy in capturing nuanced EEG patterns and delineating complex decision boundaries associated with AD diagnosis. The carefully selected feature space further enhanced the model's ability to distinguish between classes. Crucially, the GAEF model's rapid adaptation to these decision boundaries without overfitting or underfitting highlights its robustness and potential for clinical applications. With its high accuracy and ability to generalize across heterogeneous patterns, the GAEF model presents a promising tool for healthcare professionals in early and

accurate AD diagnosis. Future research directions could involve larger-scale clinical studies with diverse patient populations and longitudinal data to further refine and validate the model. Additionally, exploring the integration of multimodal data sources, such as combining EEG with other neuroimaging modalities like fNIRS, could potentially enhance the model's diagnostic capabilities, further solidifying its role in advancing AD detection and patient care.

CRediT authorship contribution statement

Chayut Bunterngchit: Conceptualization, Data curation, Methodology, Resources, Software, Validation, Visualization, Writing – original draft. **Chaowanan Jamroen:** Formal analysis, Visualization, Writing – review and editing. **Saba Aslam:** Data curation, Methodology, Visualization, Writing – review and editing. **Abdur Rasool:** Formal analysis, Methodology, Software, Validation, Visualization. **Oluwarotimi Williams Samuel:** Conceptualization, Formal analysis, Investigation, Project administration, Supervision, Validation.

Declaration of competing interest

The authors declare that they have no known competing financial interests or personal relationships that could have appeared to influence the work reported in this paper.

Data availability

The datasets used in this research are open-sourced datasets. The code is available at https://github.com/yiamcb/GAEF.

References

[1] Zhang J, Zhang Y, Wang J, Xia Y, Zhang J, Chen L. Recent advances in Alzheimer's disease: mechanisms, clinical trials and new drug development strategies. Signal Transduct Target Ther 2024;9(1).
[2] Sweidan J, El-Yacoubi MA, Rigaud A-S. Explainability of CNN-based Alzheimer's disease detection from online handwriting. Sci Rep 2024;14(1).
[3] Skaria AP. The economic and societal burden of Alzheimer disease: managed care considerations. Am J Manag Care 2022;28(Suppl 10):S188–96.
[4] Tarawneh R, Holtzman DM. The clinical problem of symptomatic Alzheimer disease and mild cognitive impairment. Cold Spring Harb Perspect Med 2012;2(5). a006148–a006148.
[5] Merlo SA, Belluscio MA, Pedreira ME, Merlo E. Memory persistence: from fundamental mechanisms to translational opportunities. Transl Psychiatry 2024;14(1).
[6] Han Z, Yang X, Huang S. Sleep deprivation: A risk factor for the pathogenesis and progression of Alzheimer's disease. Heliyon 2024;10(7):e28819.
[7] Duara R, Barker W. Heterogeneity in Alzheimer's disease diagnosis and progression rates: Implications for therapeutic trials. Neurotherapeutics 2022;19(1):8–25.
[8] Yokoi T. Alzheimer's disease is a disorder of consciousness. Gerontol Geriatr Med 2023;9.
[9] Jack CR, Bennett DA, Blennow K, Carrillo MC, Dunn B, Haeberlein SB, Holtzman DM, Jagust W, Jessen F, Karlawish J, Liu E, Molinuevo JL, Montine T, Phelps C, Rankin KP, Rowe CC, Scheltens P, Siemers E, Snyder HM, Sperling R, Elliott C, Masliah E, Ryan L, Silverberg N. NIA-AA research framework: Toward a biological definition of Alzheimer's disease. Alzheimer's & Dement 2018;14(4):535–62.
[10] Arevalo-Rodriguez I, Smailagic N, Roqué-Figuls M, Ciapponi A, Sanchez-Perez E, Giannakou A, Pedraza OL, Bonfill Cosp X, Cullum S. Mini-mental state examination (MMSE) for the early detection of dementia in people with mild cognitive impairment (MCI). Cochrane Database Syst Rev 2021;2021(7).
[11] Jia X, Wang Z, Huang F, Su C, Du W, Jiang H, Wang H, Wang J, Wang F, Su W, Xiao H, Wang Y, Zhang B. A comparison of the mini-mental state examination (MMSE) with the montreal cognitive assessment (MoCA) for mild cognitive impairment screening in Chinese middle-aged and older population: a cross-sectional study. BMC Psychiatry 2021;21(1).
[12] Kabiri S, Jameie M, Balali P, Adib Moradi S, Sanjari Moghaddam H, Aghamollaii V, Harirchian MH. Trail making test could predict impairment in cognitive domains in patients with multiple sclerosis: A study of diagnostic accuracy. Arch Clin Neuropsychol 2022;38(1):37–48.
[13] Bunterngchit C, Wang J, Su J, Wang Y, Liu S, Hou Z-G. Temporal attention fusion network with custom loss function for EEG–fNIRS classification. J Neural Eng 2024;21(6):066016.
[14] Upadhyay P, Tomar P, Yadav SP. Advancements in Alzheimer's disease classification using deep learning frameworks for multimodal neuroimaging: A comprehensive review. Comput Electr Eng 2024;120:109796.
[15] Bunterngchit C, Wang J, Hou Z-G. Simultaneous EEG-fNIRS data classification through selective channel representation and spectrogram imaging. IEEE J Transl Eng Health Med 2024;12:600–12.
[16] van Nifterick AM, Gouw AA, van Kesteren RE, Scheltens P, Stam CJ, de Haan W. A multiscale brain network model links Alzheimer's disease-mediated neuronal hyperactivity to large-scale oscillatory slowing. Alzheimer's Res & Ther 2022;14(1).
[17] Miltiadous A, Gionanidis E, Tzimourta KD, Giannakeas N, Tzallas AT. DICE-Net: A novel convolution-transformer architecture for Alzheimer detection in EEG signals. IEEE Access 2023;11:71840–58.
[18] Bunterngchit C, Wang J, Su J, Wang Y, Liu S, Hou Z-G. Enhanced cross-subject classification of hybrid EEG-fNIRS data using the simplified multimodal transformer network. In: Mahmud M, Doborjeh M, Wong K, Leung ACS, Doborjeh Z, Tanveer M, editors. Neural information processing. Singapore: Springer Nature Singapore; 2025, p. 300–13.
[19] Gautam P, Singh M. A multidimensional U-net architecture for Alzheimer's disease classification using T1 weighted brain structural MRI. Comput Electr Eng 2025;128:110687.
[20] Chen Y, Wang H, Zhang D, Zhang L, Tao L. Multi-feature fusion learning for Alzheimer's disease prediction using EEG signals in resting state. Front Neurosci 2023;17.
[21] Lalawat RS, Kushwaha N, Bajaj V, padhy PK. NeuroFormer: A deep learning framework for Alzheimer's detection using EEG signals. IEEE J Biomed Health Informatics 2025;1–9.
[22] Tan E, Troller-Renfree SV, Morales S, Buzzell GA, McSweeney M, Antúnez M, Fox NA. Theta activity and cognitive functioning: Integrating evidence from resting-state and task-related developmental electroencephalography (EEG) research. Dev Cogn Neurosci 2024;67:101404.
[23] Puri DV, Nalbalwar SL, Nandgaonkar AB, Gawande JP, Wagh A. Automatic detection of Alzheimer's disease from EEG signals using low-complexity orthogonal wavelet filter banks. Biomed Signal Process Control 2023;81:104439.

[24] Sharma N, Kolekar MH, Jha K. EEG based dementia diagnosis using multi-class support vector machine with motor speed cognitive test. Biomed Signal Process Control 2021;63:102102.
[25] Safi MS, Safi SMM. Early detection of Alzheimer's disease from EEG signals using hjorth parameters. Biomed Signal Process Control 2021;65:102338.
[26] Şeker M, Özbek Y, Yener G, Özerdem MS. Complexity of EEG dynamics for early diagnosis of Alzheimer's disease using permutation entropy neuromarker. Comput Methods Programs Biomed 2021;206:106116.
[27] Miltiadous A, Tzimourta KD, Giannakeas N, Tsipouras MG, Afrantou T, Ioannidis P, Tzallas AT. Alzheimer's disease and frontotemporal dementia: A robust classification method of EEG signals and a comparison of validation methods. Diagnostics 2021;11(8):1437.
[28] Shukla A, Tiwari R, Tiwari S. Review on Alzheimer disease detection methods: Automatic pipelines and machine learning techniques. Sci 2023;5(1):13.
[29] Kachare PH, Sangle SB, Puri DV, Khubrani MM, Al-Shourbaji I. STEADYNet: Spatiotemporal EEG analysis for dementia detection using convolutional neural network. Cogn Neurodynamics 2024;18(5):3195–208.
[30] Arya AD, Verma SS, Chakarabarti P, Chakrabarti T, Elngar AA, Kamali A-M, Nami M. A systematic review on machine learning and deep learning techniques in the effective diagnosis of Alzheimer's disease. Brain Informatics 2023;10(1).
[31] Bunterngchit C, Chearanai T, Bunterngchit Y. Advanced EEG-based classification of Alzheimer's disease using CNN-LSTM-attention architecture. In: 2024 22nd International conference on research and education in mechatronics. IEEE; 2024, p. 107–12.
[32] Acharya M, Deo RC, Barua PD, Devi A, Tao X. EEGConvNeXt: A novel convolutional neural network model for automated detection of Alzheimer's disease and frontotemporal dementia using EEG signals. Comput Methods Programs Biomed 2025;262:108652.
[33] Liu Y, An L, Yang H, Ge SS. Multi-frequency EEG and multi-functional connectivity graph convolutional network based detection method of patients with Alzheimer's disease. Complex & Intell Syst 2025;11(8).
[34] Lu Y, Fei Z, Zhang J, Chen Z, Chen M, Wang C, Liu G. Graph-weighted high-dimensional information-based similarity for detecting altered brain functional connectivity in sleep apnea patients. IEEE Trans Instrum Meas 2025;74:1–10.
[35] Khatun S, Morshed BI, Bidelman GM. A single-channel EEG-based approach to detect mild cognitive impairment via speech-evoked brain responses. IEEE Trans Neural Syst Rehabil Eng 2019;27(5):1063–70.
[36] Dogan S, Baygin M, Tasci B, Loh HW, Barua PD, Tuncer T, Tan R-S, Acharya UR. Primate brain pattern-based automated Alzheimer's disease detection model using EEG signals. Cogn Neurodynamics 2022;17(3):647–59.
[37] Zhang Z, Wei Y, Rao X, Yu L, Sun W, Li R, Zhang X, Chen X, Huang X. Electroencephalographic biomarker-guided early detection of Alzheimer's disease via cortically subdivided neurodynamic PINN. Expert Syst Appl 2026;297:129353.
[38] Ruiz-Gómez S, Gómez C, Poza J, Gutiérrez-Tobal G, Tola-Arribas M, Cano M, Hornero R. Automated multiclass classification of spontaneous EEG activity in Alzheimer's disease and mild cognitive impairment. Entropy 2018;20(1):35.
[39] Araújo T, Teixeira JP, Rodrigues PM. Smart-data-driven system for Alzheimer disease detection through electroencephalographic signals. Bioengineering 2022;9(4):141.
[40] Lopes M, Cassani R, Falk TH. Using CNN saliency maps and EEG modulation spectra for improved and more interpretable machine learning-based Alzheimer's disease diagnosis. In: Zhang G, editor. Comput Intell Neurosci 2023;2023(1).
[41] Jain S, Srivastava R. Electroencephalogram (EEG) based fuzzy logic and spiking neural networks (FLSNN) for advanced multiple neurological disorder diagnosis. Brain Topogr 2025;38(3).
[42] Dharia SY, Liu Q, Smith SD, Valderrama CE. Dual-transformer cross-attention framework for Alzheimer's disease detection via dPTE-guided EEG channel selection and multi-modal integration. Biomed Signal Process Control 2026;112:108390.
[43] Miltiadous A, Tzimourta KD, Afrantou T, Ioannidis P, Grigoriadis N, Tsalikakis DG, Angelidis P, Tsipouras MG, Glavas E, Giannakeas N, Tzallas AT. A dataset of scalp EEG recordings of Alzheimer's disease, frontotemporal dementia and healthy subjects from routine EEG. Data 2023;8(6):95.
[44] Sedghizadeh MJ, Aghajan H, Vahabi Z. Brain electrophysiological recording during olfactory stimulation in mild cognitive impairment and Alzheimer disease patients: An EEG dataset. Data Brief 2023;48:109289.
[45] Vicchietti ML, Ramos FM, Betting LE, Campanharo ASLO. Computational methods of EEG signals analysis for Alzheimer's disease classification. Sci Rep 2023;13(1).
[46] Alves CL, Pineda AM, Roster K, Thielemann C, Rodrigues FA. EEG functional connectivity and deep learning for automatic diagnosis of brain disorders: Alzheimer's disease and schizophrenia. J Phys: Complex 2022;3(2):025001.
[47] Escudero J, Abásolo D, Hornero R, Espino P, López M. Analysis of electroencephalograms in Alzheimer's disease patients with multiscale entropy. Physiol Meas 2006;27(11):1091.